Supplementary Information

Carbon Tetrafluoride - Sulphur Hexafluoride Adsorption and Separation with Zirconium Metal-Organic Frameworks Decorated with Fluorinated Thiazolium Salts

Giacomo Provinciali,[a] *Giulio Bicchierai,*[a] *Zhi Fang,*[b] *Tongan Yan,*,*[c] *Lorenzo Donà,*,*[d] *Bartolomeo Civalleri,*[d] *Hongliang Huang,*[c] *Giuliano Giambastiani,*[e,f,a] *Giulia Tuci,*[a,f] *and Andrea Rossin*,*[a,f]

[a] Istituto di Chimica dei Composti Organometallici (CNR-ICCOM), Via Madonna del Piano 10, Sesto Fiorentino (Firenze), 50019, Italy. E-mail: andrea.rossin@cnr.it

[b] School of Materials Science and Engineering, Tiangong University, Tianjin 300387, China.

[c] School of Chemistry and Chemical Engineering, Tiangong University, Tianjin 300387, China. E-mail: yantongan@tiangong.edu.cn

[d] Department of Chemistry, NIS and INSTM Reference Centre, Università di Torino, Via G. Quarello 15, 10135 and Via P. Giuria 7, 10125 Torino, Italy. E-mail: lorenzo.dona@unito.it

[e] Dipartimento di Chimica "Ugo Schiff", Università di Firenze, Via della Lastruccia 3-13, 50019 Sesto Fiorentino (Firenze), Italy.

[f] Consorzio Interuniversitario Nazionale per la Scienza e Tecnologia dei Materiali (INSTM), Via G. Giusti, 9 50121 Firenze, Italy.

Synthesis and characterization of the thiazolium salts used in this work

Synthesis of 3-(4-carboxy-2-fluorobenzyl)thiazol-3-ium bromide [(HPhTz^{F})Br]

4-(bromomethyl)-3-fluorobenzoic acid ($C_8H_6BrFO_2$, FW = 233.04, 0.326 g, 1.4 mmol) and thiazole (C_3H_3NS, FW = 85.12, 0.100 g, 1.17 mmol) were dissolved in acetonitrile (8 mL). The solution was heated at 353 K for 24 h. During this time, an off-white precipitate formed. Afterwards, the solid was filtered *in vacuo* and washed with acetone (3 × 10 mL) to obtain the pure thiazolium salt (**HPhTz^{F}**)Br. Yield: 0.365 g (98%). Elemental analysis calcd. (%) for (**HPhTz^{F}**)Br, $C_{11}H_9BrFNO_2S$ (MW = 2230.6 g/mol): C 41.5, H 2.8, N 4.4, S 10.1. Elemental analysis found (%): C, 41.3; H, 2.6; N, 4.6; S, 10.0. ^{1}H-NMR [δ_H (ppm), 600 MHz, T = 298 K, DMSO-d_6]: 10.33 (s, 1H, H^{9}), 8.54 (d, $^{3}J_{H\text{-}H}$ = 3.8 Hz, 1H, H^{10}), 8.38 (d, $^{3}J_{H\text{-}H}$ = 3.8 Hz, 1H, H^{11}) 7.85 (d, $^{3}J_{H\text{-}H}$ = 7.9 Hz, 1H, H^{3}), 7.76 (d, $^{3}J_{H\text{-}H}$ = 7.9 Hz, 1H, H^{4}), 7.59 (t, $^{3}J_{H\text{-}F}$ = 7.6 Hz, 1H, H^{7}), 5.96 (s, 2H, H^{8}). ^{13}C NMR [δ_C (ppm), 226 MHz, T = 298 K, DMSO-d_6]: 166.21 (C^{1}), 161.03 (C^{9}), 159.95 (C^{2}), 137.61 (C^{10}), 134.65 (d, $^{1}J_{C\text{-}F}$ = 7.1 Hz, C^{6}), 131.76 (C^{7}), 128.03 (C^{11}), 126.36 (C^{3}), 126.05 (C^{5}), 116.84 (C^{4}), 51.98 (C^{8}). The ^{13}C NMR peaks assignments were made through a 2D ^{13}C-^{1}H HETCOR experiment. ^{19}F-NMR [δ_F (ppm), 565 MHz, T = 298 K, DMSO-d_6]: –115.91 (s). IR bands (KBr pellet, cm^{-1}, Fig. S3): 1720(vs), 1585(m), 1548(m), 1428(vs), 1407(m), 1365(m), 1276(w), 1254(s) , 1239(vs), 1206(m), 1184(vs), 1149(vs), 1094(m), 1075(s), 979(w) 924(m), 907(m), 893(m), 868(m), 853(m), 831(m), 800(s), 759(s), 726(vs), 678(w), 645(w), 619(m), 584(w), 423(w). Single crystals suitable for X-ray diffraction were grown from concentrated methanol/acetonitrile solutions left at T = 298 K upon slow evaporation.

Synthesis of 3-(4-carboxy-2-(trifluoromethyl)benzyl)thiazol-3-ium bromide [(HPhTz^{CF3})Br]

4-(bromomethyl)-3-(trifluoromethyl)benzoic acid ($C_9H_6BrF_3O_2$, FW = 283.04 g/mol, 0.396 g, 1.4 mmol) and thiazole (C_3H_3NS, FW = 85.12 g/mol, 0.100 g, 1.17 mmol) were dissolved in acetonitrile (8 mL). The solution was heated at 353 K for 24 h. During this time, an off-white precipitate formed. Afterwards, the solid was filtered *in vacuo* and washed with acetone (3 × 10 mL) to obtain the pure thiazolium salt (**HPhTz^{CF3}**)Br. Yield: 0.365 g (79%). Elemental analysis calcd. (%) for (**HPhTz^{CF3}**)Br, $C_{12}H_9BrF_3NO_2S$ (FW = 368.17 g/mol): C 39.1, H 2.5, N 3.8, S 8.7. Elemental analysis found (%): C, 39.2; H, 2.6; N, 3.9; S, 9.0.

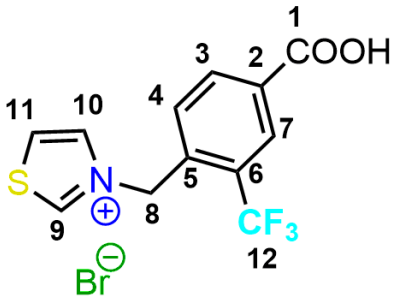

^{1}H-NMR [δ_H (ppm), 600 MHz, T = 298 K, DMSO-d_6]: 10.36 (s, 1H, H^9), 8.56 (d, $^3J_{H\text{-}H}$ = 3.1 Hz, 1H, H^{10}), 8.45 (d, $^3J_{H\text{-}H}$ = 3.1 Hz, 1H, H^{11}), 8.28 (s, 1H, H^7), 8.25 (d, $^3J_{H\text{-}H}$ = 8.0 Hz, 1H, H^3), 7.36 (d, $^3J_{H\text{-}H}$ = 8.0 Hz, 1H, H^4), 6.14 (s, 2H, H^8). ^{13}C-NMR [δ_C (ppm), 226 MHz, T = 298 K, DMSO-d_6]: 166.02 (C^1), 161.80 (C^9), 137.93 (C^{10}), 136.56 (C^3), 134.52 (C^2), 132.38 (C^5), 131.11 (C^4), 128.09 (C^{11}), 127.60 (C^6), 127.48 (C^7), 124.00 (q, $^1J_{C\text{-}F}$ = 272.6 Hz, C^{12}), 54.48 (C^8). The ^{13}C NMR peaks assignments were made through a 2D ^{13}C-^{1}H HETCOR experiment. ^{19}F-NMR [δ_F (ppm), 565 MHz, T = 298 K, DMSO-d_6]: –59.13 (s). IR bands (KBr pellet, cm^{-1}, Fig. S3): 1712(s), 1618(m), 1549(w), 1416(m), 1384(s), 1311(s), 1279(m), 1268(m), 1227(vs), 1179(s), 1158(m), 1127(vs), 1048(s), 919(w), 911(w), 851(s), 756(s), 740(s), 725(m), 625(w), 593(m), 522(w), 457(w). Single crystals suitable for X-ray diffraction were grown from concentrated water solutions left at T = 298 K upon slow evaporation.

Single crystal X-ray diffraction analysis

Single crystal X-ray diffraction data for (**HPhTz^{F}**)Br and (**HPhTz^{CF3}**)Br as monohydrate adducts were collected at low temperature (T = 100 K) on a Bruker APEX-II CCD diffractometer equipped with a sealed X-ray source (Cu Kα, λ = 1.5418 Å or Mo Kα, λ = 0.71073 Å). Direct methods, as implemented in Sir2014,[1] were used to solve the crystal and molecular structure. Structure refinement was then performed by full-matrix least-squares against F^2, as implemented in SHELXL-2018.[2] All the non-hydrogen atoms were refined anisotropically, while all the hydrogen atoms in the cation were fixed in calculated positions (adopting the riding model) and refined isotropically with $U_{iso} = 1.2U_{eq}$(C) (C = carbon atom to which the H atom is bound). The hydrogen atoms on the water molecule were located from the residual electron density maps and refined isotropically with $U_{iso} = 1.5U_{eq}$(O) (O = oxygen atom to which the H atom is bound). The geometrical calculations were performed by PARST97,[3] while Fig. S1 and S2 were produced with the program ORTEP3.[4] CCDC 2448941 and 2448942 contain the supplementary crystallographic data for this paper. These data can be obtained free of charge from The Cambridge Crystallographic Data Centre *via* https://www.ccdc.cam.ac.uk/structures/. Tables S1 and S2 collect the main experimental details and crystallographic data.

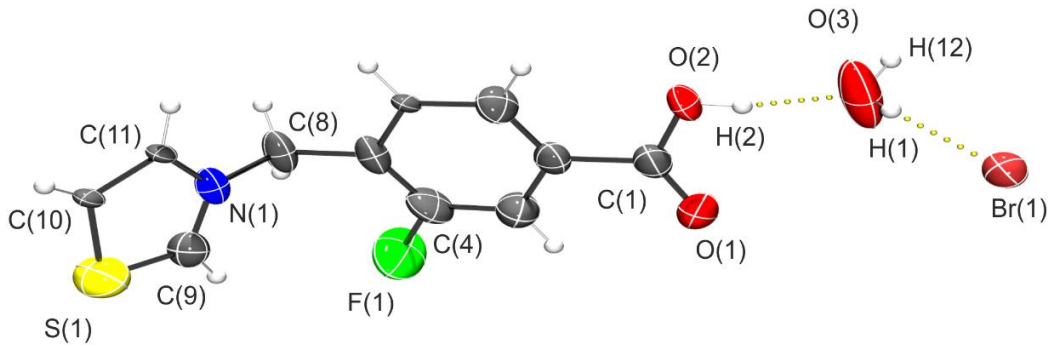

Fig. S1. ORTEP drawing of (**HPhTz^{F}**)Br · H_2O at 70% probability level. Selected bond lengths (Å) and angles (°): C(1)-O(1) 1.201(6); C(1)-O(2) 1.320(6); C(4)-F(1) 1.359(6); C(9)-S(1) 1.663(5); C(10)-S(1) 1.770(4); C(8)-N(1) 1.478(5); C(9)-N(1) 1.331(6); O(3)-H(1) 0.86(12); O(3)-H(12) 0.74(11); O(1)-C(1)-O(2) 124.9(4); C(9)-N(1)-C(8) 123.2(4); C(11)-N(1)-C(8) 123.2(4); H(1)-O(3)-H(12) 111(10). Hydrogen bonds [d(D-H···A)]: O(2)-H(2)···O(3) 2.533(5); O(3)-H(1)...Br(1) 3.209(4).

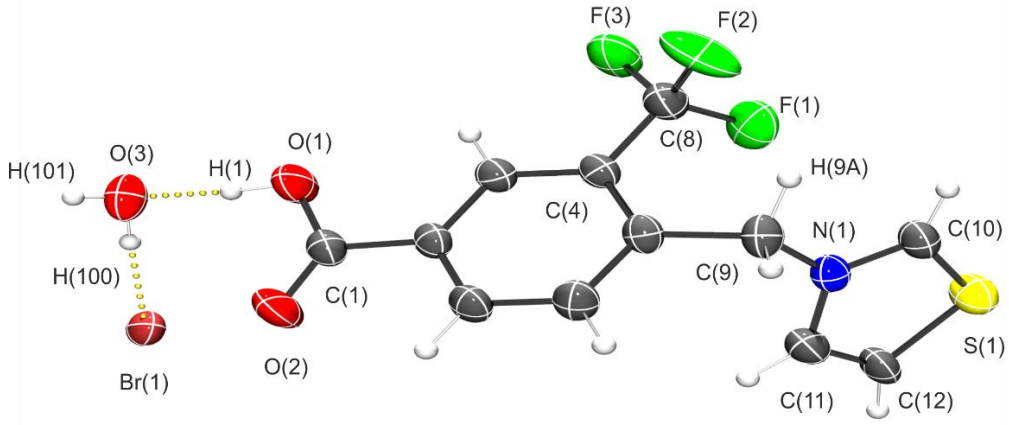

Fig. S2. ORTEP drawing of (**HPhTz^{CF3}**)Br · H_2O at 70% probability level. Selected bond lengths (Å) and angles (°): C(1)-O(1) 1.3232(19); C(1)-O(2) 1.2110(19); C(4)-C(8) 1.510(2); C(8)-F(1) 1.3508(19); C(8)-F(2) 1.3416(19); C(8)-F(3) 1.3359(19); C(9)-N(1) 1.4891(19); C(10)-N(1) 1.3321(19); C(10)-S(1) 1.6752(16); O(1)-H(1) 0.91(3); O(3)-H(100) 0.89(3); O(3)-H(101) 0.78(3); O(2)-C(1)-O(1)124.15(14); C(10)-N(1)-C(9) 123.13(12); H(100)-O(3)-H(101) 105(3). Hydrogen bonds [d(D-H···A)]: C(9)-H(9A)···F(2) 3.137(2); O(1)-H(1)···O(3) 2.5631(17); O(3)-H(100)···Br(1) 3.2699(13).

Table S1. Main crystallographic data and structure refinement details for (**HPhTz^{F}**)Br· H_2O.

Formula	C_{11} H_{11} Br F N O_3 S
M [g mol^{-1}]	336.18
T [K]	100
Colour, habit	Colorless, prisms
Size [mm^3]	0.02 × 0.03 × 0.05
Crystallographic system	Monoclinic
Space group	$P2_1/c$
Z	4
a [Å]	13.6968(6)
b [Å]	12.6423(6)
c [Å]	7.7593(3)
β [°]	100.0900(10)
V [Å^3]	1322.81(10)
F(000)	672
μ (Cu Kα) [mm^{-1}]	5.851
D_{calc} [g cm^{-3}]	1.688
θ range for collection [°]	3.277 to 72.318
h, k, l ranges for collection	$-16 \le h \le 16$,
	$-13 \le k \le 15$,
	$-9 \le l \le 9$
Measured reflns	20869
Unique, observed reflns	2601
Completeness [%]	99.7 (to θ = 67.679°)
R_{int}	0.0528
Data / restraints / parameters	2601 / 6 / 158
R1, wR2 [$I > 2\sigma(I)$]	0.0608, 0.1618
R1, wR2 (all data)	0.0618, 0.1625
Gof on F^2	1.025
Max peak, min hole [e Å^{-3}]	4.149, −1.498

Table S2. Main crystallographic data and structure refinement details for (**HPhTz^{CF3}**)Br · H_2O.

Formula	C_{12} H_{11} Br F_3 N O_3 S
M [g mol^{-1}]	386.19
T [K]	100
Colour, habit	Colorless, prisms
Size [mm^3]	0.04 × 0.04 × 0.07
Crystallographic system	Monoclinic
Space group	$P2_1/c$
Z	4
a [Å]	12.6925(12)
b [Å]	8.1562(5)
c [Å]	14.9774(13)
β [°]	108.615(3)
V [Å^3]	1469.4(2)
F(000)	768
μ (Mo Kα) [mm^{-1}]	2.980
D_{calc} [g cm^{-3}]	1.746
θ range for collection [°]	2.829 to 36.359
h, k, l ranges for collection	$-16 \le h \le 21$,
	$-13 \le k \le 13$,
	$-24 \le l \le 20$
Measured reflns	33785
Unique, observed reflns	7130
Completeness [%]	99.9 (to θ = 25.242°)
R_{int}	0.0679
Data / restraints / parameters	7130 / 0 / 198
$R1$, w$R2$ [$I > 2\sigma(I)$]	0.0385, 0.0950
$R1$, w$R2$ (all data)	0.0554, 0.1022
Gof on F^2	1.060
Max peak, min hole [e Å^{-3}]	0.890, −1.124

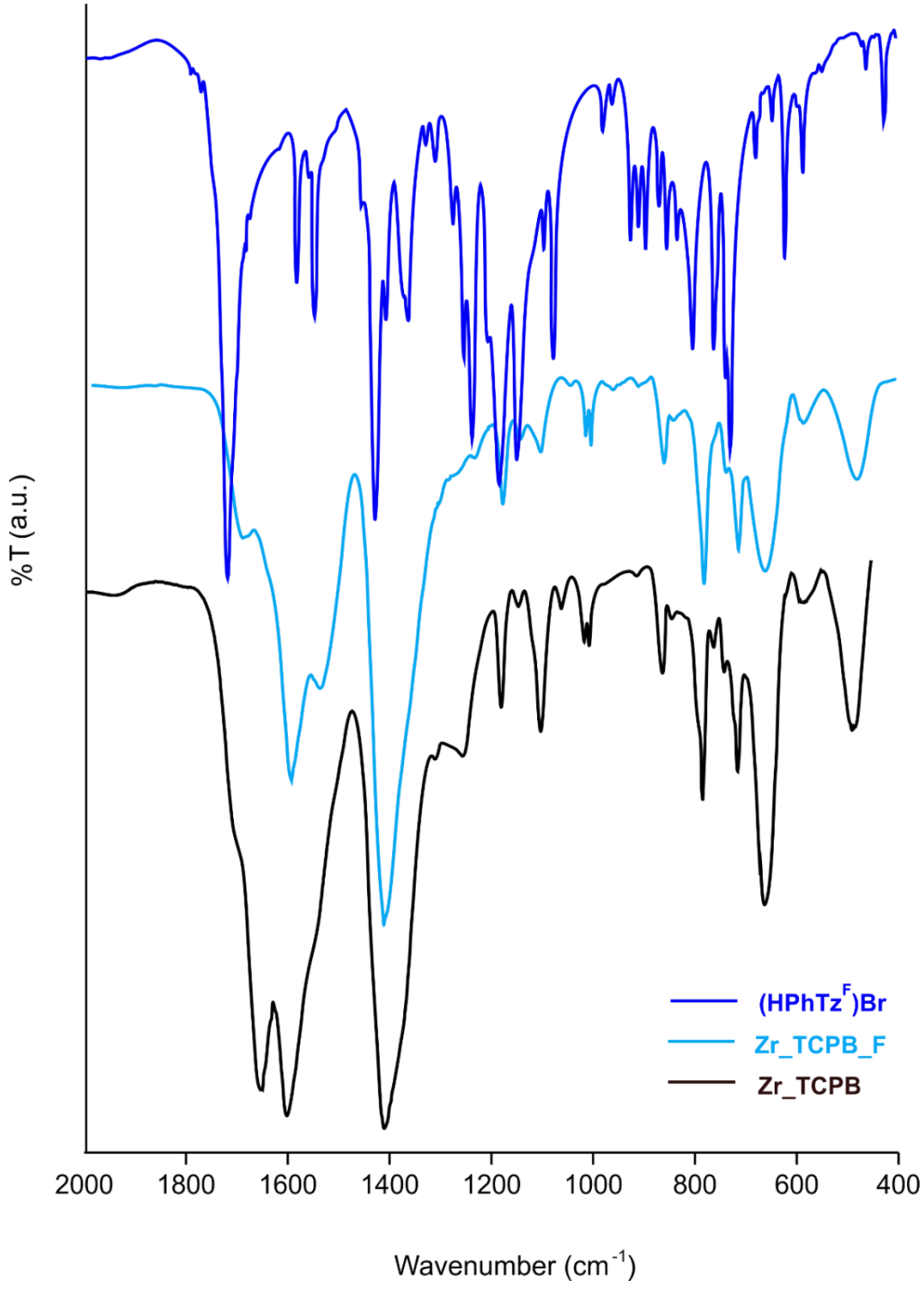

Fig. S3. Infrared spectra (KBr, T = 298 K, 2000-400 cm^{-1}) of **Zr_TCPB_F** and its constitutive parts **Zr_TCPB** and (**HPhTz^{F}**)Br at comparison.

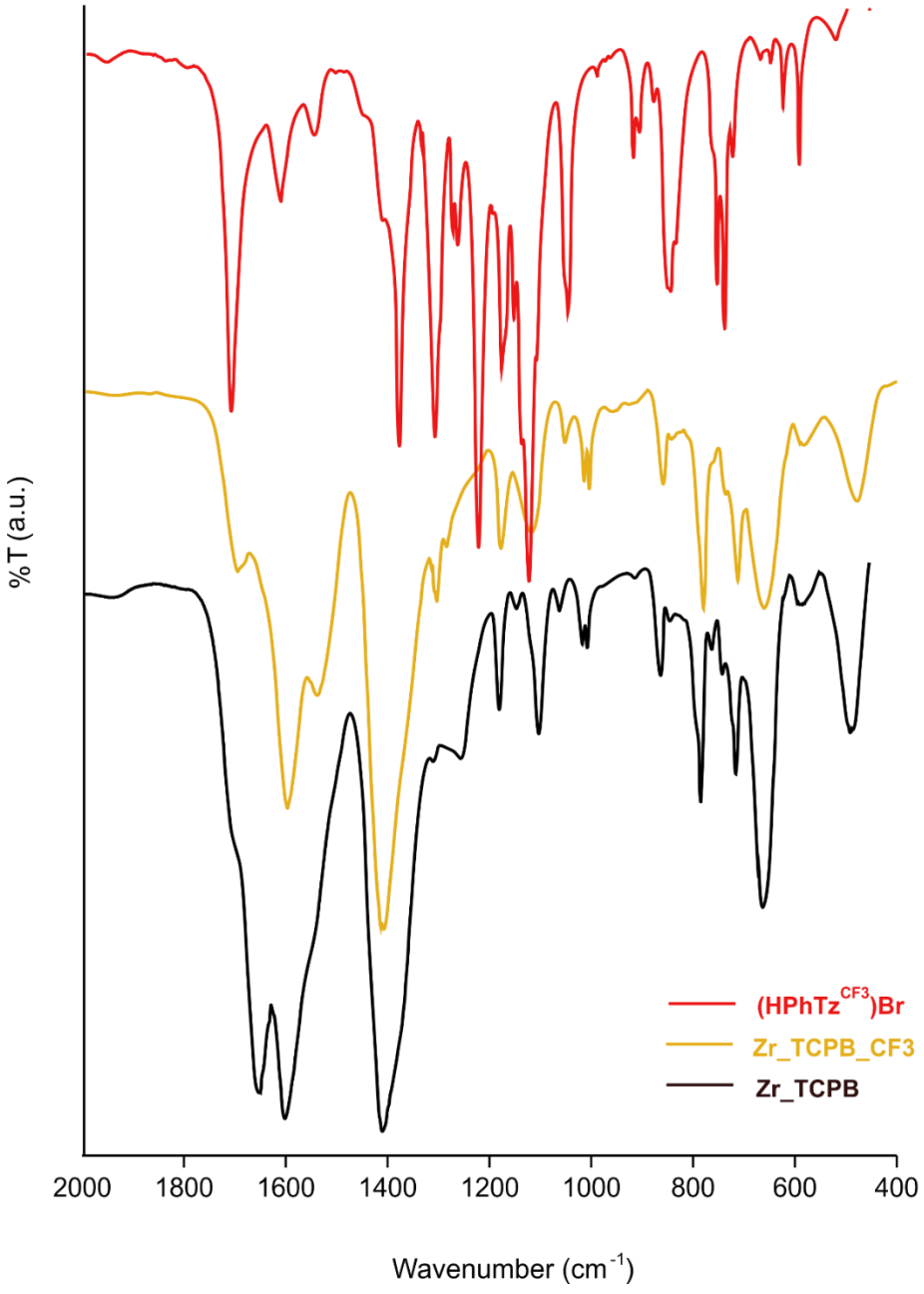

Fig. S4. Infrared spectra (KBr, T = 298 K, 2000-400 cm^{-1}) of **Zr_TCPB_CF3** and its constitutive parts **Zr_TCPB** and (**HPhTz^{CF3}**)Br at comparison.

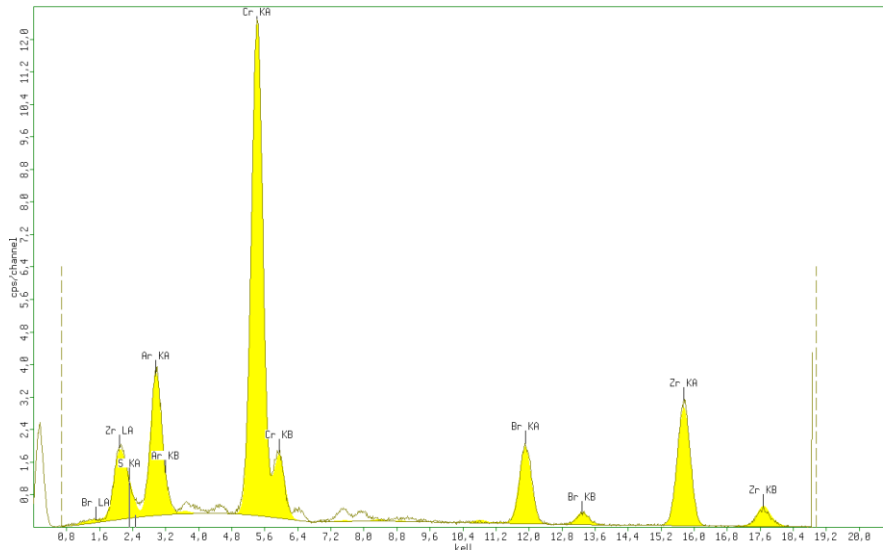

Fig. S5. X-ray fluorescence spectra of powdered samples of thermally activated **Zr_TCPB_F** with the corresponding elemental analysis. The signals of chromium are due to the chemical nature of the X-ray source anode, while the signal of argon descends from the fact that the spectra were acquired in air.

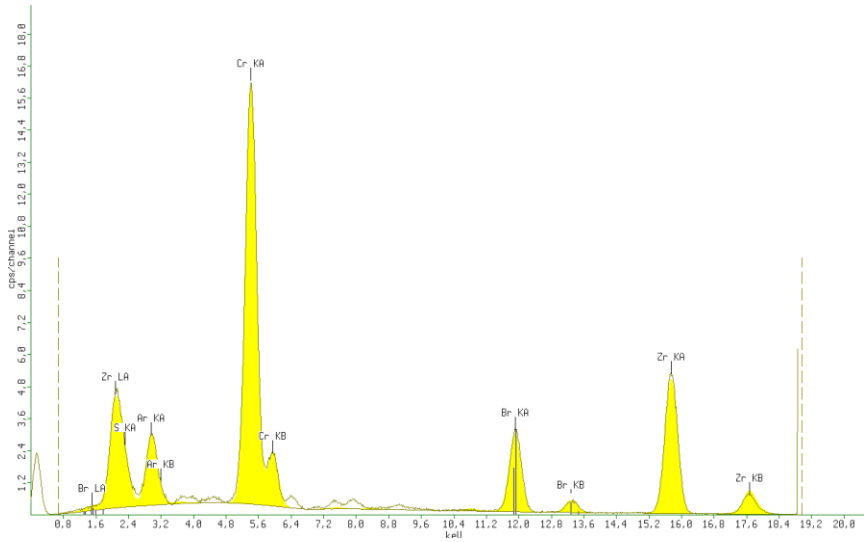

Fig. S6. X-ray fluorescence spectra of powdered samples of thermally activated **Zr_TCPB_CF3** with the corresponding elemental analysis. The signals of chromium are due to the chemical nature of the X-ray source anode, while the signal of argon descends from the fact that the spectra were acquired in air.

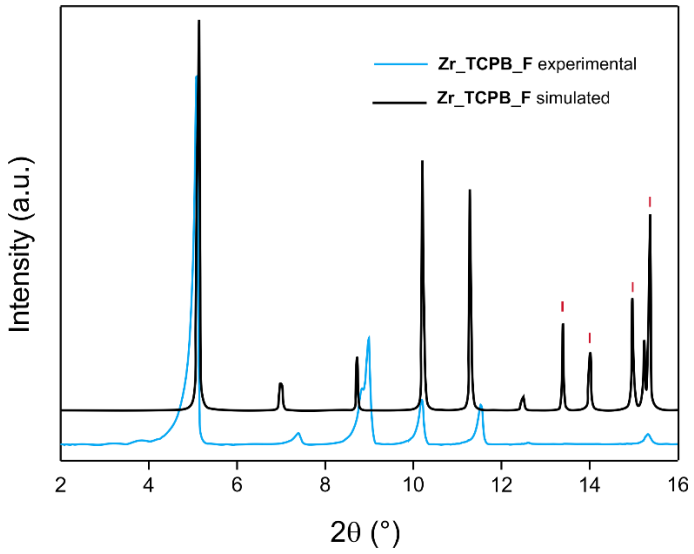

Fig. S7. Comparison between the experimental (light blue curve) and the theoretically-derived (black curve) X-ray powder pattern of **Zr_TCPB_F** (2°-16° 2θ region). The extra peaks (red ticks) in the latter stem from the lower crystal symmetry of the *finite* computational model with respect to that of the real crystal.

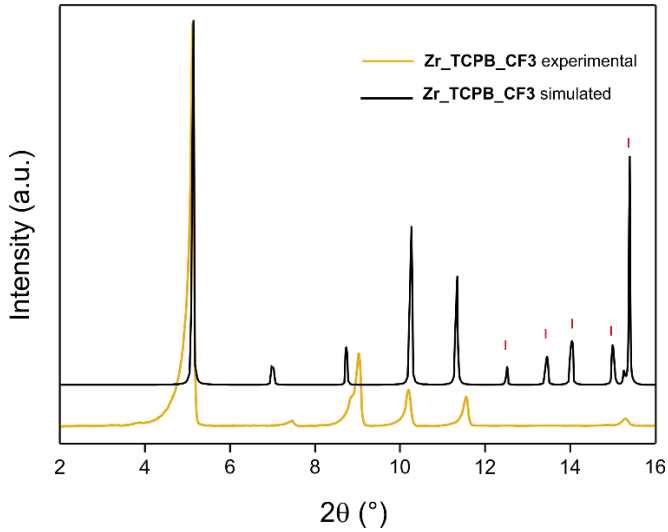

Fig. S8. Comparison between the experimental (orange curve) and the theoretically-derived (black curve) X-ray powder pattern of **Zr_TCPB_CF3** (2°-16° 2θ region). The extra peaks (red ticks) in the latter stem from the lower crystal symmetry of the *finite* computational model with respect to that of the real crystal.

Linker quantification in the MIXMOFs through combined ^{1}H and ^{19}F NMR spectroscopy of the digested solid

An accurate estimation of the amount of the two linkers present in **Zr_TCPB_F** and **Zr_TCPB_CF3** was performed using ^{1}H (τ = 5 s; 32 scans) and ^{19}F (τ = 10 s; 32 scans) NMR spectroscopy in the presence of the internal standard 2,6-difluorobenzoic acid (DFB, $C_7H_4F_2O_2$, FW = 158.1), following a methodology similar to that reported by Farha *et al.* in 2013.[5] 0.005 g of MIXMOF and 0.005 g of DFB were dissolved in 0.75 mL of DMSO-d_6 and 20 µL D_2SO_4/D_2O (Sigma Aldrich). The moles of H_4TCPB and fluorinated linker were calculated from ^{1}H and ^{19}F signal integration against the standard, respectively, and taking into account the different number of ^{1}H or ^{19}F nuclei in the two molecules. The [H_4TCPB/fluorinated linker] molar ratio was then exploited to derive the MIXMOF minimal formula.

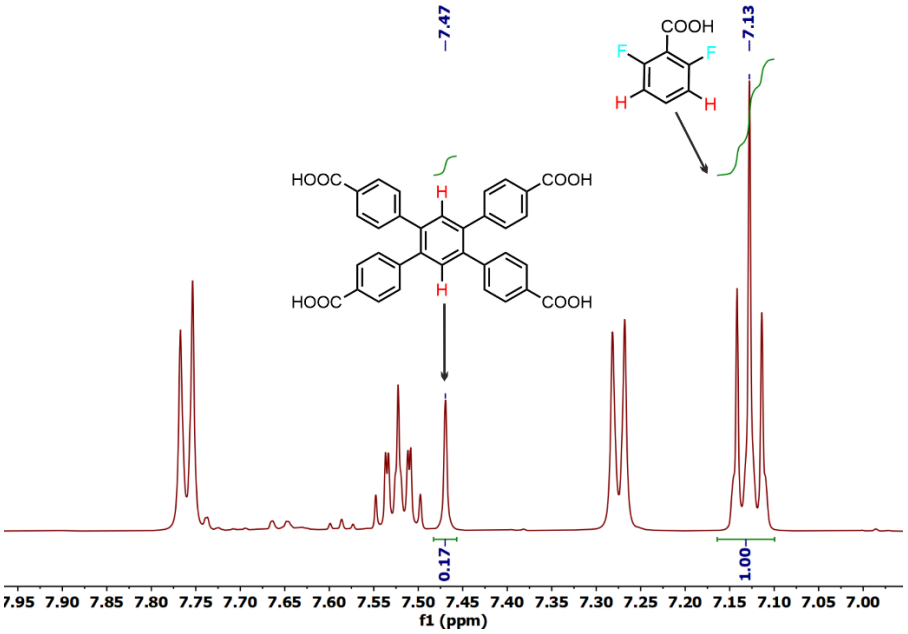

Fig. S9. Magnification of the aromatic region of the ^{1}H NMR spectrum (600 MHz, D_2SO_4/D_2O/DMSO-d_6, 298 K) of digested **Zr_TCPB_F** in the presence of DFB (internal standard).

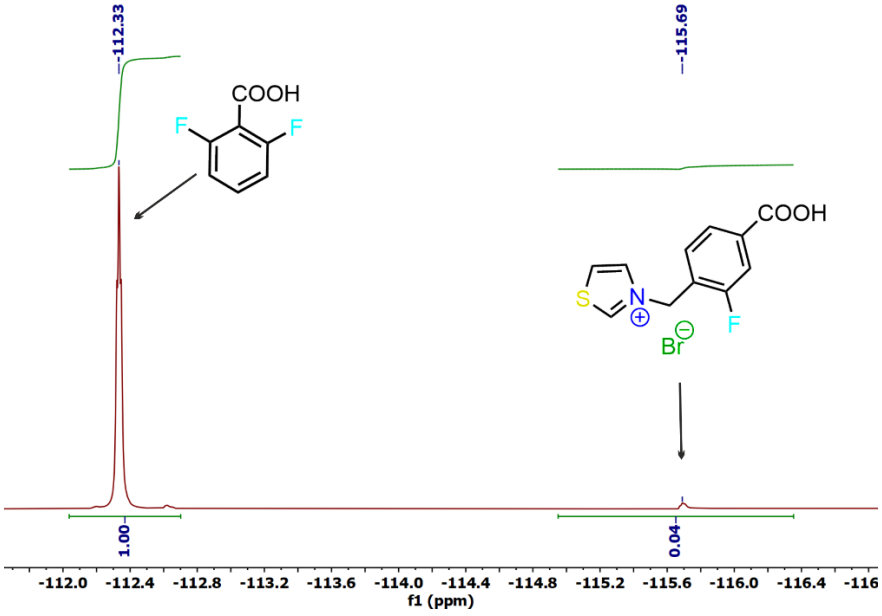

Fig. S10. ^{19}F NMR spectrum (565 MHz, D_2SO_4/D_2O/DMSO-d_6, 298 K) of digested **Zr_TCPB_F** in the presence of DFB (internal standard).

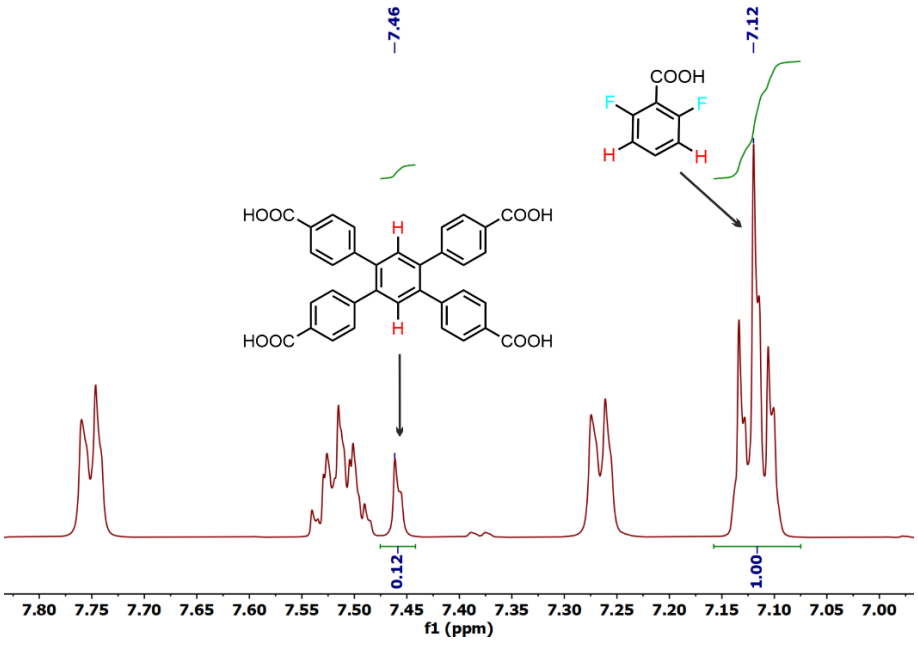

Fig. S11. Magnification of the aromatic region of the ^{1}H NMR spectrum (600 MHz, D_2SO_4/D_2O/DMSO-d_6, 298 K) of digested **Zr_TCPB_CF3** in the presence of DFB (internal standard).

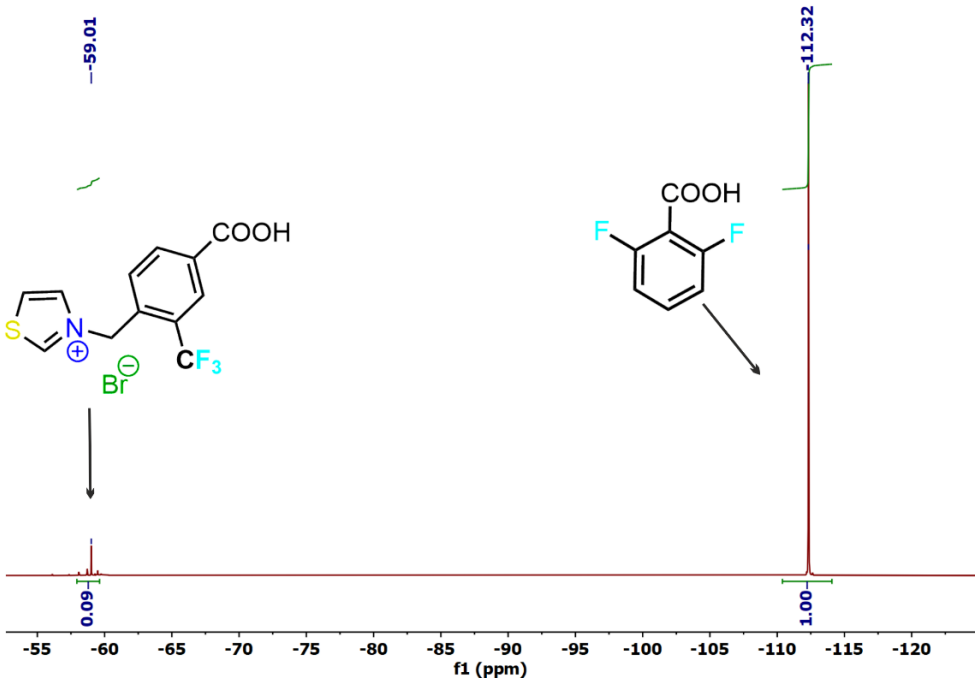

Fig. S12. ^{19}F NMR spectrum (565 MHz, D_2SO_4/D_2O/DMSO-d_6, 298 K) of digested **Zr_TCPB_CF3** in the presence of DFB (internal standard).

Zr_TCPB_F: mmol DFB = 5/158.1 = 0.032. From the ^1H NMR integral values: mmol H_4TCPB = 0.032 × 0.17 = 0.0054; from the ^{19}F NMR integral values: mmol **HPhTz^F**= (0.032 × 0.04)/0.5 = 0.0027. Thus: [H_4TCPB/ **HPhTz^F**] molar ratio = 2.

Zr_TCPB_CF3: mmol DFB = 5/158.1 = 0.032. From the ^1H NMR integral values: mmol H_4TCPB = 0.032 × 0.12 = 0.0038; from the ^{19}F NMR integral values: mmol **HPhTz^{CF3}**= (0.032 × 0.03)/0.5 = 0.0019. Thus: [H_4TCPB/ **HPhTz^{CF3}**] molar ratio = 2.

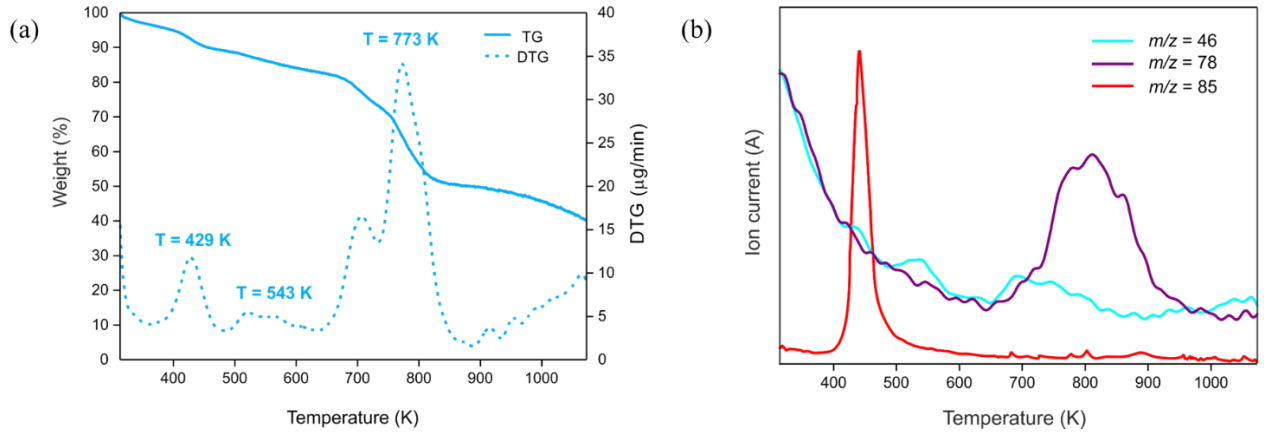

Fig. S13. TG-DTG traces (a) and related mass spectrometry peaks (b) of **Zr_TCPB_F**.

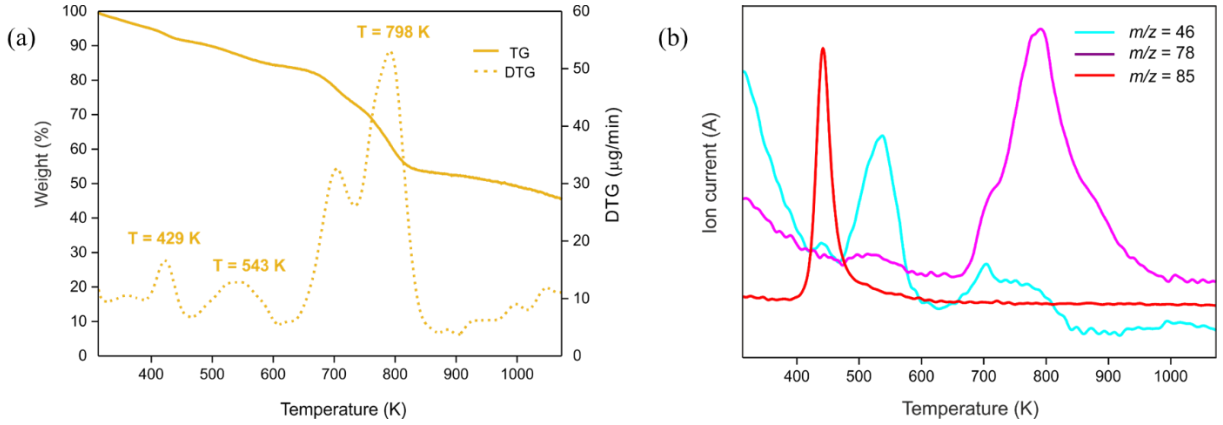

Fig. S14. TG-DTG traces (a) and related mass spectrometry peaks (b) of **Zr_TCPB_CF3**.

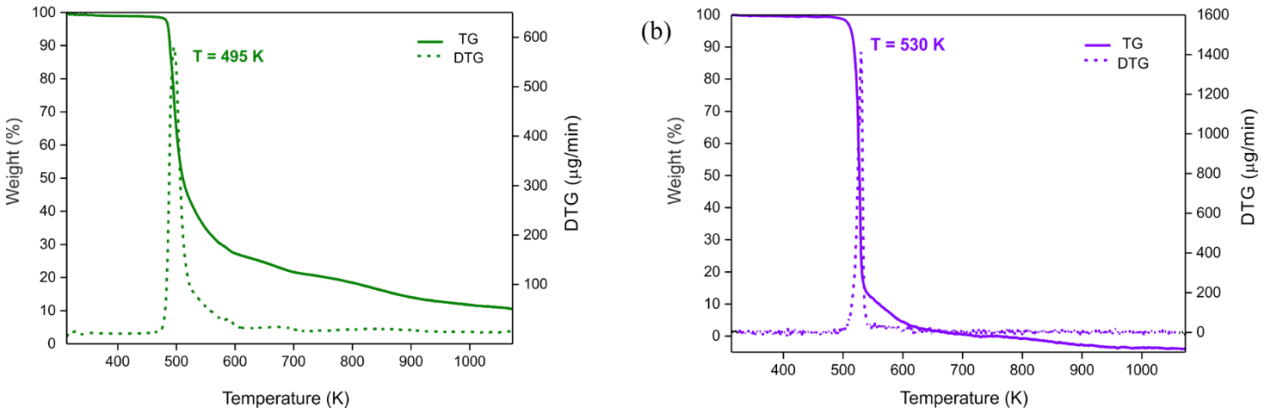

Fig. S15. TG-DTG traces of (a) (**HPhTz^{F}**)Br and (b) (**HPhTz^{CF3}**)Br.

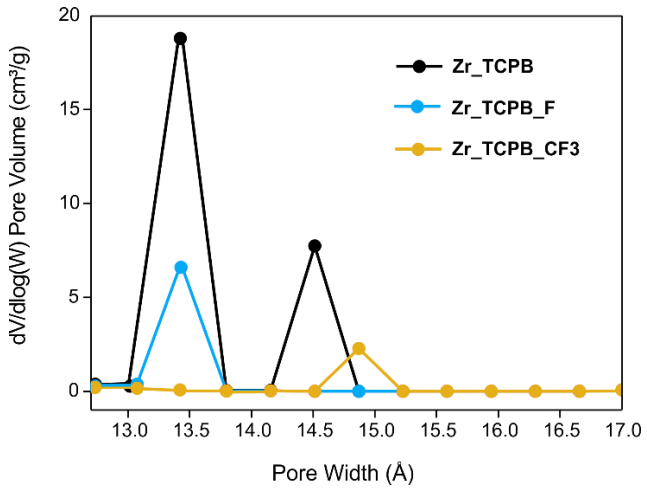

Fig. S16. Micropore size distribution (NLDFT method – Tarazona approximation, cylindrical pore shape) of **Zr_TCPB**, **Zr_TCPB_F** and **Zr_TCPB_CF3** at comparison.

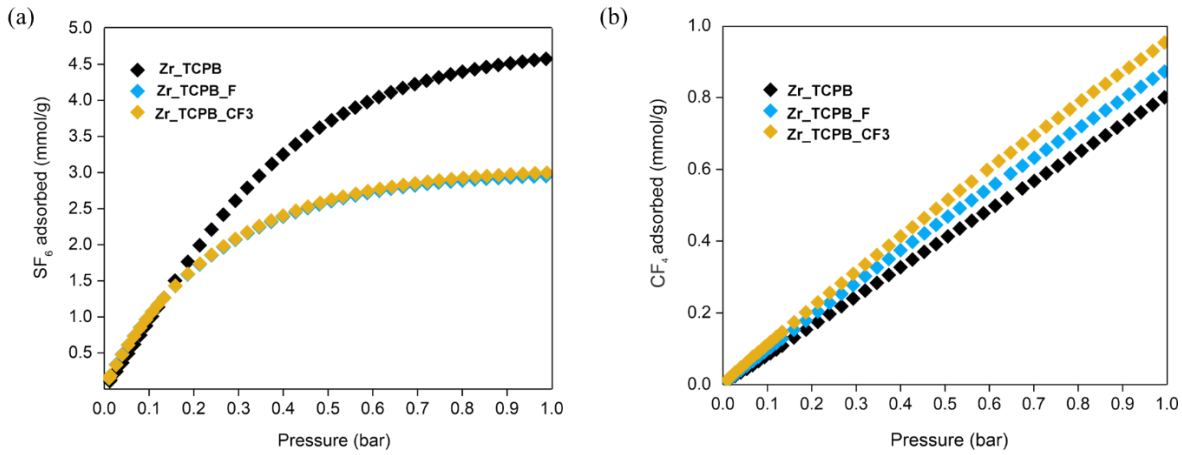

Fig. S17. Collective (a) SF_6 and (b) CF_4 adsorption isotherms at T = 273 K for **Zr_TCPB**, **Zr_TCPB_F** and **Zr_TCPB_CF3** in comparison.

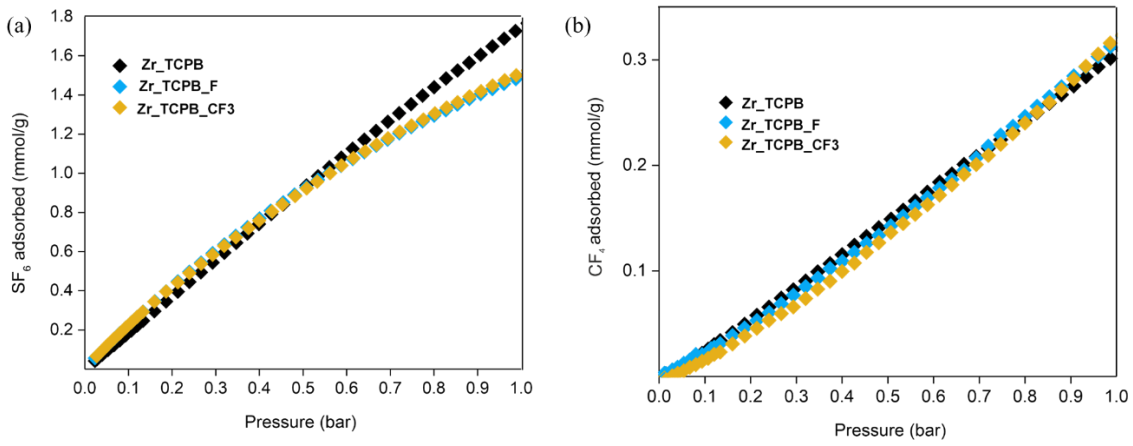

Fig. S18. Collective (a) SF_6 and (b) CF_4 adsorption isotherms at T = 323 K for **Zr_TCPB**, **Zr_TCPB_F** and **Zr_TCPB_CF3** in comparison.

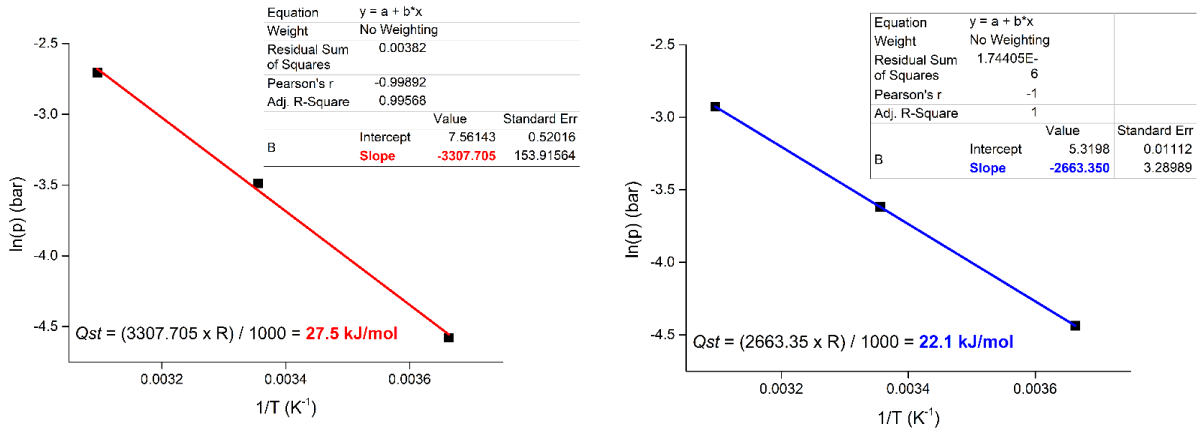

Fig. S19. Linear fitting of the differential form of the Clausius-Clapeyron equation for SF_6 (left; coverage = 2.1 wt.%) and CF_4 (right; coverage = 0.09 wt.%) adsorption in **Zr_TCPB_F** at the three temperatures of 273, 298 and 323 K.

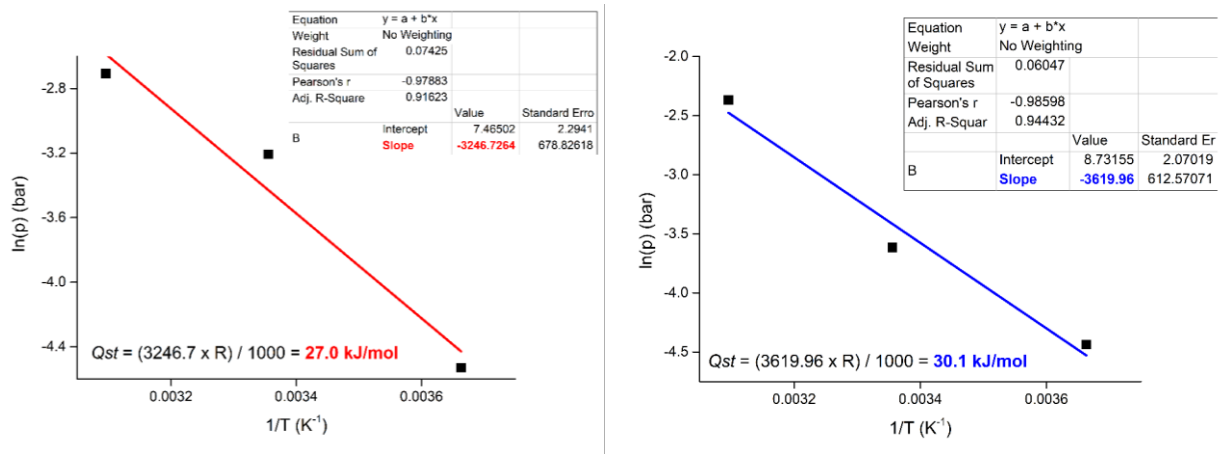

Fig. S20. Linear fitting of the differential form of the Clausius-Clapeyron equation for SF_6 (left; coverage = 2.2 wt.%) and CF_4 (right; coverage = 0.09 wt.%) adsorption in **Zr_TCPB_CF3** at the three temperatures of 273, 298 and 323 K.

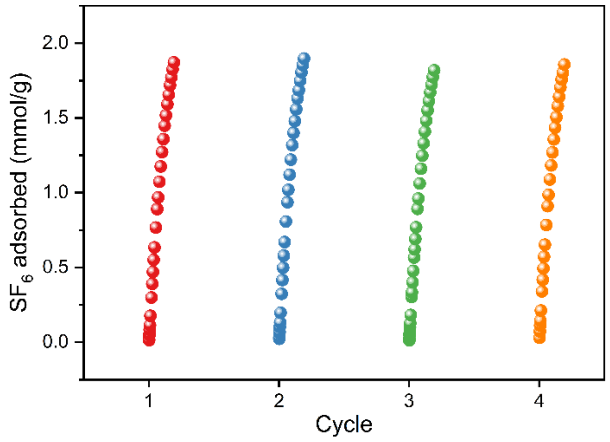

Fig. S21. Repeated SF_6 adsorption/desorption tests on **Zr_TCPB_F** at ambient temperature.

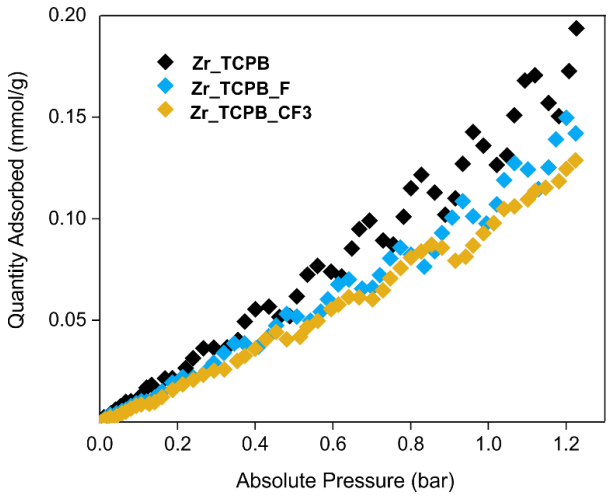

Fig. S22. N_2 adsorption isotherms collected at T = 298 K of **Zr_TCPB**, **Zr_TCPB_F** and **Zr_TCPB_CF3** at comparison.

Table S3. Main fitting parameters (IAST) for the isotherms collected in this work.

	Zr_TCPB	**Zr_TCPB_F**	**Zr_TCPB_CF3**
CF_4 model	BET	Henry	BET
RMSE value (CF_4)	0.0021	0.0025	0.0102
Fitting parameters (CF_4)	M = 17.63 K_A = 0.027 K_B = 0.062	K_H = 0.728	M = 7.97 K_A = 0.037 K_B = 0.204
SF_6 model	Quadratic	BET	Quadratic
RMSE value (SF_6)	0.013	0.0031	0.0093
Fitting parameters (SF_6)	M = 2.68 K_a = 1.22 K_b = 1.46	M = 4.69 K_A = 1.02 K_B = –0.03	M = 1.97 K_a = 1.824 K_b = 2.474
N_2 model	Henry	Henry	Henry
RMSE value (N_2)	0.0085	0.0058	0.0041
Fitting parameters (N_2)	K_H = 0.135	K_H = 0.108	K_H = 0.096

Refer to the pyIAST webpage (https://pyiast.readthedocs.io/en/latest/#) for the detailed mathematical description of these models.

Dynamic breakthrough experiments

The breakthrough experiments were conducted using a multi-component adsorption breakthrough curve analyzer (BSD-MAB) under ambient temperature and pressure conditions (T = 298 K, p_{tot} = 1 bar). Prior to measurement, **Zr_TCPB_F** and **Zr_TCPB_CF3** were vacuum degassed at room temperature for 24 hours. Subsequently, approximately 800 mg of sample was loaded into a quartz glass tube (Φ4 mm × 180 mm) as an adsorption column and purged for 2 hours under a He flow (30 mL/min). Finally, the binary gas mixture of SF_6/CF_4 (volume ratio 50/50) with a total flow rate of 2 mL/min was introduced into the adsorption column for breakthrough testing. The outlet gas is monitored using a gas chromatograph (GC-9860, Shanghai S·Sun Information Technology Co. Ltd.) equipped with a Thermal Conductivity Detector (TCD). Chromatography column parameters: Porapak Q (5 m, 60/80 mesh); Inlet temperature: 493 K; Injection pressure: 170 kPa; TCD temperature: 393 K; Column oven temperature: 373 K.

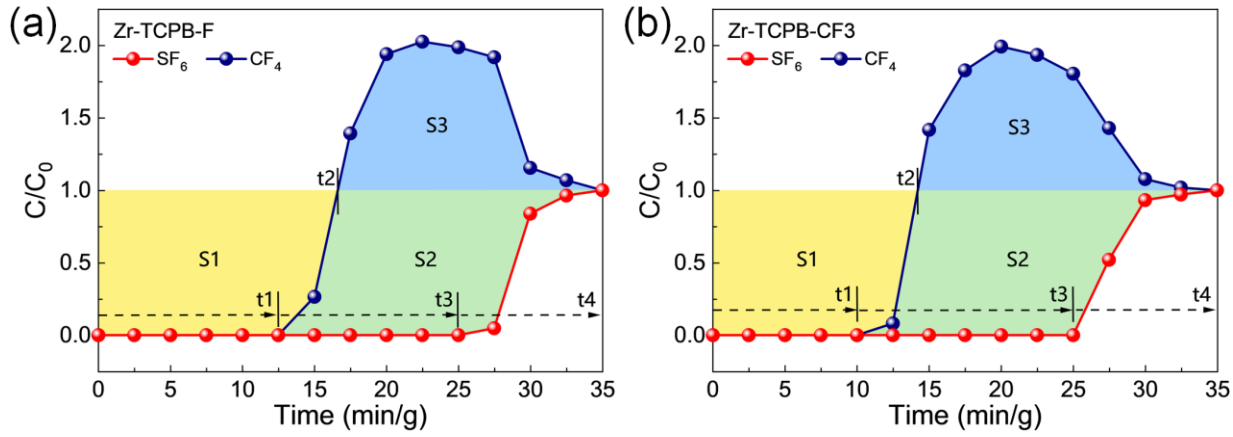

Fig. S23. Breakthrough experiments using (a) **Zr_TCPB_F** and (b) **Zr_TCPB_CF3** for the SF_6/CF_4 (50/50, v/v) mixture at T = 298 K and p_{tot} = 1 bar for the calculation of the dynamic separation factors.

The SF_6 adsorption capacity in the breakthrough experiment is the sum of the duration t1 before breakthrough and the adsorption capacity of mass transfer zone (t1–t2). The SF_6 adsorption capacity can be obtained by the sum of the areas S1 and S2. Since $C/C_0 > 1.0$, the CF_4 adsorption capacity is obtained by the difference of the area integral between S1 and S3. A similar method has been widely used to estimate the breakthrough experiment adsorption capacity.[6-8] The maximum capture amount of SF_6 and CF_4 per separation process is calculated as:

$$Q_{\mathrm{SF_6}} = \frac{V \cdot c\%}{22.4 \cdot m} \times \int_0^{t_4} (C_0 - C_i)\ dt = \frac{V \cdot c\%}{22.4 \cdot m} \times (S_1 + S_2)$$

(Equation S1)

$$Q_{CF_4} = \frac{V \cdot c\%}{22.4 \cdot m} \times \left\{ \int_0^{t_2} (C_0 - C_i)\ dt - \left[\int_{t_1}^{t_4} C_i\ dt - \int_{t_1}^{t_2} C_i\ dt - \int_{t_2}^{t_4} C_0\ dt \right] \right\} = \frac{V \cdot c\%}{22.4 \cdot m} \times (S_1 - S_3)$$

(Equation S2)

where V is the total flow rate (ml/min); m is the sample mass; c% is gas volume content (SF_6 or CF_4), C_0 is the inlet gas concentration for gas i (SF_6 or CF_4). The separation factor can be similarly calculated as:

$$\text{Separation factor} = \frac{Q_{\mathrm{SF_6}}}{Q_{CF_4}} = \frac{(S_1 + S_2)}{(S_1 - S_3)}$$

(Equation S3)

Table S4. Comparison of the SF_6 and CF_4 adsorption performance of **Zr_TCPB**, **Zr_TCPB_F** and **Zr_TCPB_CF3** with other Zr^{IV} MOFs from the literature.

MOF	SSA [m^2/g]	Qst (SF_6) [kJ/mol]	SF_6 adsorbed* [mmol/g]	Qst (CF_4) [kJ/mol]	CF_4 adsorbed* [mmol/g]	Reference
Zr_TCPB	1406	24.9	3.0	21.9	0.5	This work
Zr_TCPB_F	1141	27.5	2.2	22.1	0.7	This work
Zr_TCPB_CF3	1126	25.1	2.5	30.1	0.5	This work
UiO-66	1333	33.0	1.4	32.0	0.7	[9/10]
UiO-66-Br	759	35.0	1.1	30.0	0.6	[10]
UiO-66-Br2	616	45.0	0.8	40.0	0.7	[10]
UiO-66-Cl	752	32.0	1.0	28.0	0.6	[10]
UiO-66-I	819	38.0	1.4	31.0	0.7	[10]
UiO-66-NH2	938	32.0	1.7	27.0	0.8	[10]
UiO-66-NO2	774	35.0	1.3	28.0	0.7	[10]
UiO-67	2411	20.0	8.9	--	--	[11]

* at ambient temperature (298 K) and pressure (1 atm).

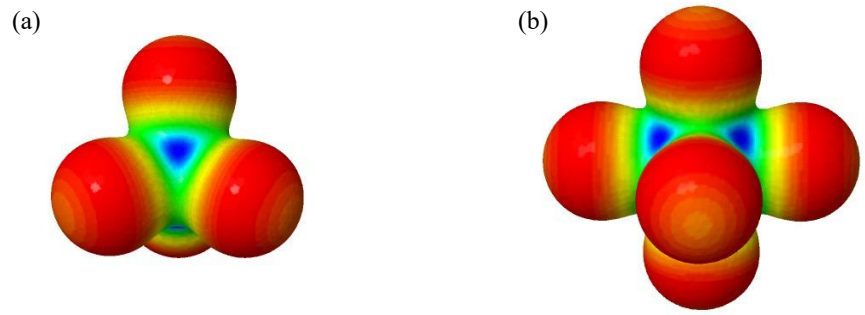

Fig. S24. Electrostatic potential (ESP) map of (a) CF_4 and (b) SF_6 computed at the PBEsol0-3c level of theory with an isovalue of 0.05 a.u. Positive regions in blue and negative regions in red.

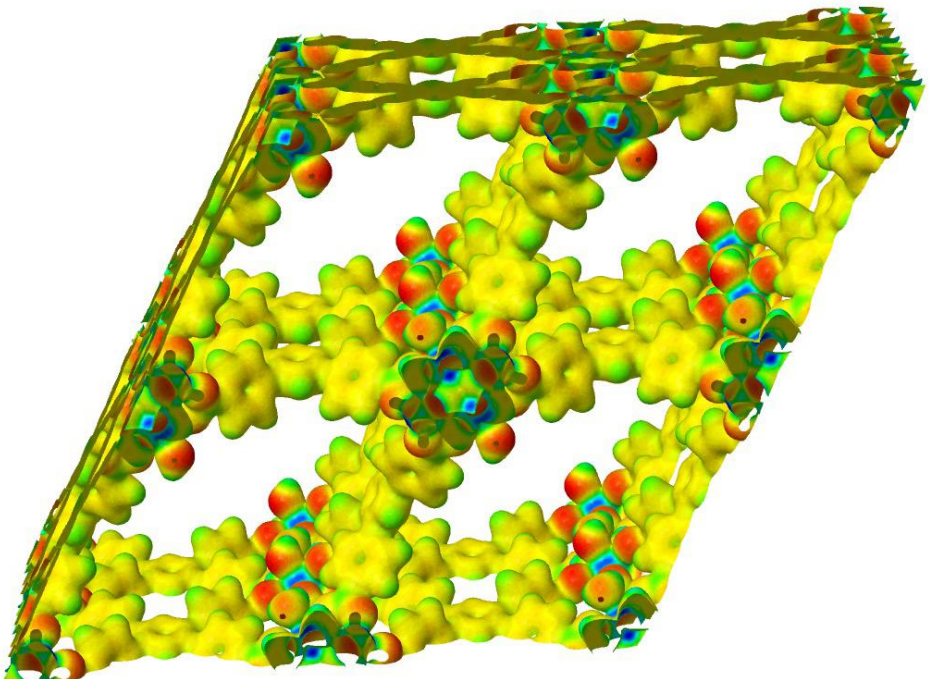

Fig. S25. Electrostatic potential (ESP) map of **Zr_TCPB** computed at the PBEsol0-3c level of theory with an isovalue of 0.05 a.u. Positive regions in blue and negative regions in red.

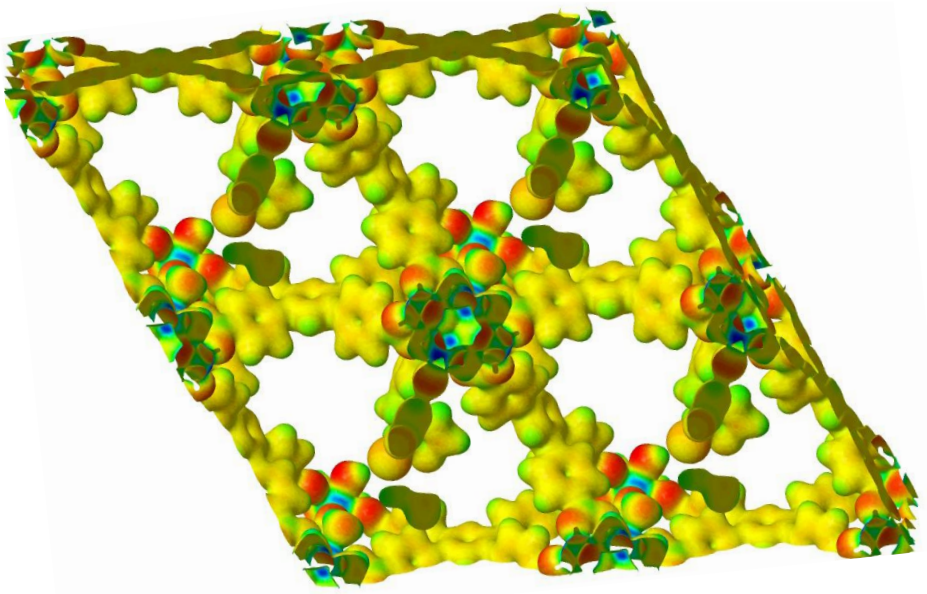

Fig. S26. Electrostatic potential (ESP) map of **Zr_TCPB_F** computed at the PBEsol0-3c level of theory with an isovalue of 0.05 a.u. Positive regions in blue and negative regions in red.

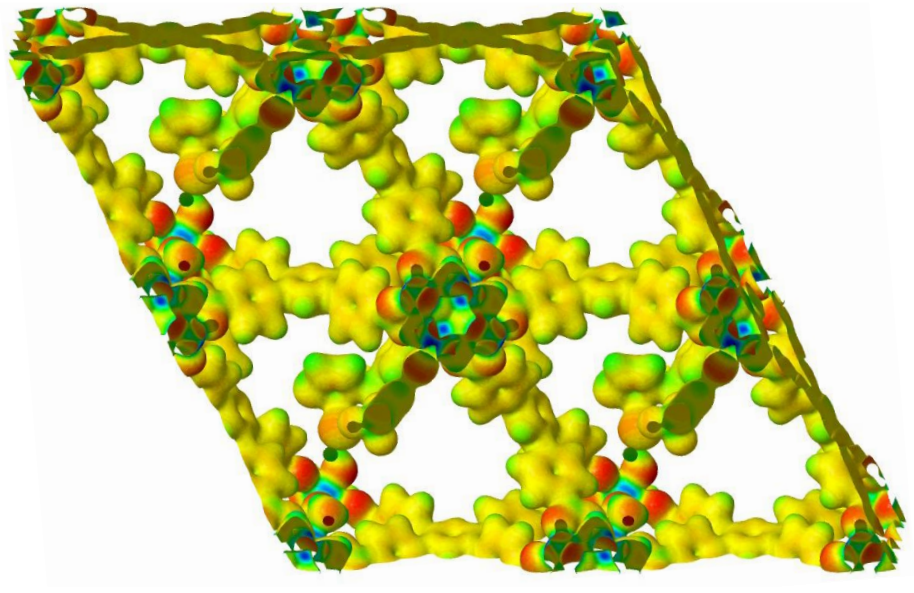

Fig. S27. Electrostatic potential (ESP) map of **Zr_TCPB_CF$_3$** computed at the PBEsol0-3c level of theory with an isovalue of 0.05 a.u. Positive regions in blue and negative regions in red.

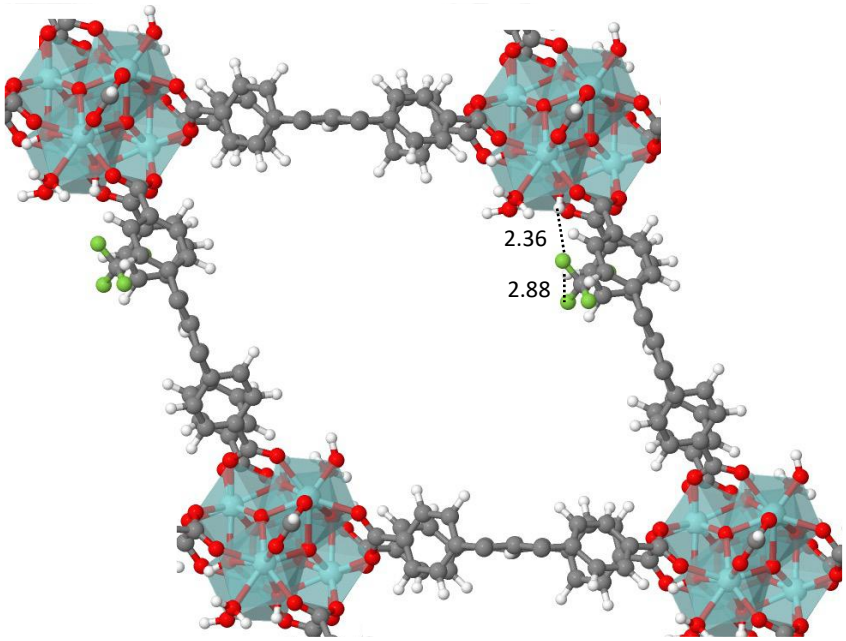

Fig. S28. Optimized geometry of [CF_4@**Zr_TCPB**] (portion of the crystal structure only, for the sake of clarity). Main gas-framework distances reported (Å).

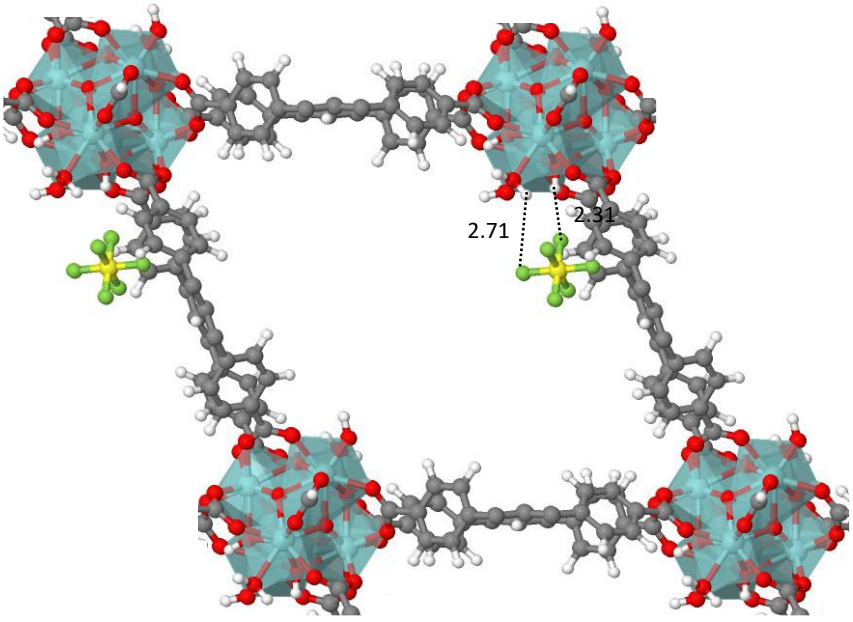

Fig. S29. Optimized geometry of [SF_6@**Zr_TCPB**] (portion of the crystal structure only, for the sake of clarity). Main gas-framework distances reported (Å).

Table S5. Comparison between calculated PBEsol0-3c interaction energies (kJ/mol) for CF_4 in **Zr_TCPB**, **Zr_TCPB_F** and **Zr_TCPB_CF3** and the experimental isosteric heats of adsorption.

MOF	PBEsol0-3c	Exp.
Zr_TCPB	-26.06	-21.9
Zr_TCPB_F	-17.78	-22.1
Zr_TCPB_CF3	-29.16	-30.1

Table S6. Comparison between calculated PBEsol0-3c interaction energies (kJ/mol) for SF_6 in **Zr_TCPB**, **Zr_TCPB_F** and **Zr_TCPB_CF3** and the experimental isosteric heats of adsorption.

MOF	PBEsol0-3c	Exp.
Zr_TCPB	-27.33	-24.9
Zr_TCPB_F	-48.46	-27.5
Zr_TCPB_CF3	-22.82	-27.0

References

1. M. C. Burla, R. Caliandro, B. Carrozzini, G. L. Cascarano, C. Cuocci, C. Giacovazzo, M. Mallamo, A. Mazzone and G. Polidori, *J. Appl. Cryst.*, 2015, **48**, 306–309.
2. G. Sheldrick, *Acta Cryst.* , 2015, **C71**, 3–8.
3. M. Nardelli, *Comp. Chem.*, 1983, **7**, 95–98.
4. L. Farrugia, *J. Appl. Cryst.*, 1997, **30**, 565.
5. P. Deria, J. E. Mondloch, E. Tylianakis, P. Ghosh, W. Bury, R. Q. Snurr, J. T. Hupp and O. K. Farha, *J. Am. Chem. Soc.*, 2013, **135**, 16801–16804.
6. C. He, P. Zhang, Y. Wang, Y. Zhang, T. Hu, L. Li and J. Li, *Sep. Purif. Technol.*, 2023, **304**, 122318.
7. H. Zeng, X.-J. Xie, Y. Wang, D. Luo, R.-J. Wei, W. Lu and D. Li, *Chem. Sci.*, 2022, **13**, 12876–12882.
8. L. Zhang, K. Jiang, L. Yang, L. Li, E. Hu, L. Yang, K. Shao, H. Xing, Y. Cui, Y. Yang, B. Li, B. Chen and G. Qian, *Angew. Chem. Int. Ed.*, 2021, **60**, 15995–16002.
9. M.-B. Kim, T.-U. Yoon, D.-Y. Hong, S.-Y. Kim, S.-J. Lee, S.-I. Kim, S.-K. Lee, J.-S. Chang and Y.-S. Bae, *Chem. Eng. J.*, 2015, **276**, 315–321.
10. M.-B. Kim, K.-M. Kim, T.-H. Kim, T.-U. Yoon, E.-J. Kim, J.-H. Kim and Y.-S. Bae, *Chem. Eng. J.*, 2018, **339**, 223–229.
11. M.-B. Kim, T.-H. Kim, T.-U. Yoon, J. H. Kang, J.-H. Kim and Y.-S. Bae, *J. Ind. Eng. Chem.*, 2020, **84**, 179–184.